IEEE Access
Multidisciplinary ⋮ Rapid Review ⋮ Open Access Journal

Received February 2, 2019, accepted February 24, 2019, date of publication March 1, 2019, date of current version December 26, 2019.

*Digital Object Identifier 10.1109/ACCESS.2019.2902411*

# Flexible Power Control for Wireless Power Transmission System With Unfixed Receiver Position

**HAN LIU[1], XUELIANG HUANG[2,3], (Member, IEEE), DARIUSZ CZARKOWSKI[4], (Member, IEEE), LINLIN TAN[2,3], JIACHENG LI[2,3], MING ZHANG[2,3], AND ZHENXING ZHANG[2,3]**

[1]College of Energy and Electrical Engineering, Hohai University, Nanjing 210098, China
[2]School of Electrical Engineering, Southeast University, Nanjing 210096, China
[3]Key Laboratory of Smart Grid Technology and Equipment in Jiangsu Province, Zhenjiang 212000, China
[4]Department of Electrical and Computer Engineering, NYU Tandon School of Engineering, Brooklyn, NY 11201, USA

Corresponding author: Linlin Tan (tanlinlin@seu.edu.cn)

This work was supported in part by the State Grid Corporation Science and Technology Project Funding (Selection of Wireless Charging Frequency for Electric Vehicles and Its Impact on Environment), in part by the National Key R&D Project under Grant 2018YFB0106300, in part by the National Natural Science Foundation of China under Grant 51777028, in part by the Scientific Research Foundation of the Graduate School of Southeast University under Grant YBJJ1728, in part by the Postgraduate Research and Practice Innovation Program of Jiangsu Province under Grant KYCX17-0088, and in part by the China Scholarship Council.

**ABSTRACT** To improve the stability of receiving power in the wireless power transmission system with unfixed receiving position, a flexible power control strategy without the measurement in secondary side and the wireless communication between primary and secondary sides is proposed. The circuit model of a multiphase resonant inverter (MPRI) with cascaded intercell transformers (ICTs) is developed. The output voltage control strategy of the MPRI is introduced based on the iterative summation method for trigonometric functions. The circuit model of the system is derived to deduce the expressions for the key parameters. Considering the cascaded ICTs and the inductor–capacitor–capacitor (*LCC*) compensation circuit in the primary side, the design method of the compensation parameters is proposed based on the circuit model of the MPRI. After synthesizing the online monitoring, parameter pre-calculation, prediction of several conditions, and online learning, the flexible power control strategy is put forward for the wireless power transmission system with unfixed receiver position. Without the auxiliary positioning methods, the measurement in the secondary side, or the wireless communication between primary and secondary sides, the recognition of the load access and exit, as well as the power stabilization control after access, are realized. Finally, the theoretical analyses and the control strategy are validated by experiments.

**INDEX TERMS** Wireless power transmission, multiphase resonant inverter, unfixed receiver position, power stabilization, flexible power control.

## I. INTRODUCTION

Wireless power transmission (WPT) technology has received much attention in recent decades due to its convenience and safety. It is beneficial for power consumption equipment to be independent of the electric cables. The technology has been widely applied in the fields of consumer electronics [1], smart home [2], implant medical devices [3], electric vehicles [4], sensors in smart grid [5], rail transits [6] and drones. In [1], a 6.78 MHz resonant wireless power transfer (WPT) system with a 5 W fully integrated power receiver is introduced. An asymmetric wireless power transfer (WPT) system for a 150 watt LED TV is proposed in [2]. An implantable magnetic coupling resonate WPT system by integrating with metasurface for biological applications is presented in [3]. The advances in stationary and dynamic wireless charging of EVs are reviewed in [4]. The concept of the domino-resonator WPT system is applied in energy harvest from the ac magnetic field around the high-voltage cable to be transmitted wirelessly to power an online monitoring system in high-voltage transmission tower in [5]. The Design and fabrication of a 1-MW inductive power transfer system is proposed for a high-speed train in [6].

The research hotspots of WPT are mainly high frequency inverter [7], [8], energy couplers [2], [9], compensation circuits [4], [10], power rate improvement [6],

The associate editor coordinating the review of this manuscript and approving it for publication was Taufik Abrao.

system efficiency optimization [11], [12], electromagnetic compatibility (EMC) [13] and power stabilization control [14]. A voltage equalizer is proposed by combining wireless power transfer and a voltage multiplier for series-connected energy storage cells in [8]. A coil structure is proposed to minimize the coupling among the transmitters and generate a three-dimensional magnetic field in [9]. A comprehensive investigation on system topologies and characteristics is conducted in [10]. An efficiency optimization method is proposed to improve the system efficiency for the low-speed application scenarios of dynamic charging in [11]. The compact resonant reactive shielding coil topology is presented for reducing electromagnetic field in [13]. The coordinated control of two source voltages is applied to solve the power fluctuation of load in [14]. In a large number of WPT applications, the load (secondary side) is usually at unfixed receiving position or moving state. Such as the dynamic wireless power transfer or static-dynamic hybrid wireless power transfer, they are proposed to power wirelessly for the moving objects or the frequent position changing objects with tiny battery or no battery. The best state is to maintain the balance between the wirelessly receiving power and consuming power. The load is fixed or changes in a very tiny area which can be ignored. The main parameter which influences the system performance is the changing receiving position. The misalignment between the primary and secondary sides is variable, which causes mutual inductance fluctuations and the system characteristics including the receiving power and the system efficiency unstable.

In order to improve stabilization of the system performance, the DD coil structure is applied to promote the lateral misalignment tolerance in dynamic wireless power transfer system in [15]. In the WPT system with voltage power source and LC compensation circuit in primary side, the current in primary side is high when the coupling between the primary and secondary sides is weak. The LCC compensation circuit in primary side is presented to maintain the constant current and prevent the over current in primary side in [16]. In [12], the parity–time symmetric circuit based on the nonlinear gain saturation element is investigated, which results in a stable system efficiency even when the coupling coefficient changes widely. In [17], the topology conversion method in primary side is proposed to improve the receiving power stabilization in the dynamic wireless charging system. In [18], the auxiliary circuit is applied to realize the power control in the WPT system with multi-load and multi-frequency. In [7], the CC-CV (constant current and constant voltage) control of the battery charging for EVs (electric vehicles) is achieved based on a new type high frequency inverter with inter-cell transformers (ICTs, also named coupled inductors). The series compensation topology is applied in both primary side and the secondary side in [7]. Because of the unconsidered equivalent leakage inductance of the ICTs in compensation circuit, the optimal normalized operation frequency needs to be optimized and changed. In most research of the wireless power transfer, the compensation circuit is designed firstly and operation frequency is fixed during the operation process. The equivalent leakage inductance of the ICTs is taken into consideration in the parameter design of the compensation circuit to fix the operation frequency in this paper. The multi-phase resonant inverter (MPRI) [7], [19], [20] is a new branch of the inverters for the wireless power transfer system and has great potentialities. The output power can also be controlled without the DC-DC converter in the input side. In addition, the higher power rate can be realized by using the devices with lower rated current and lower price according to this topology.

In order to realize the optimization and control of receiving power and efficiency in a WPT system, the variation of characteristics in the load side (secondary side) is usually tested in secondary side and sent to the primary side through a wireless communication method. Based on the concept of measurement in secondary side and wireless communication, the frequency and power tracking method is proposed to control the receiving power in paper [21]. The closed loop control of the system is achieved after receiving the voltage of the battery and the pulse width in secondary side through the wireless communication method in paper [22]. In paper [23], the front-end monitoring method in WPT system of multiple loads is proposed without the wireless communication system, which is beneficial for decreasing the system cost and the system complexity.

To solve the issue of the power stabilization caused by frequent change of the receiver position in a WPT system for movable load, the flexible power control strategy for the wireless power transmission system with unfixed receiver position is investigated. In Section II, the circuit model of the MPRI with the cascaded ICTs is derived. Using an iterative summation method for trigonometric functions, the expression of the output voltage of the MPRI as a function of the number of phases and the maximum phase difference is deduced. According to the circuit model of the MPRI, the control method of the output voltage of the MPRI based on the adjustment of the maximum phase difference is introduced. In Section III, the circuit model of the WPT system is developed and the design method of the compensation circuit parameters in primary side is proposed based on the circuit model of the MPRI. The expressions for system parameters including the output current of the MPRI, the receiving power and the system efficiency about the number of phases, the maximum phase difference and the mutual inductance are deduced. In Section IV, for achieving the recognition of access and exit as well as the power stabilization control after access, the flexible power control strategy for the wireless power transmission system with unfixed receiver position is presented according to the online monitoring of the key parameters, pre-calculation of the inner parameters, prediction of several conditions, and the online learning. The theoretical analyses and the control strategy are validated by experiments in Section V and the conclusions are provided in Section VI.

## II. CIRCUIT ANALYSIS OF THE MPRI WITH THE CASCADED ICTS

The structure of the MPRI with the cascaded ICTs is proposed in [7]. In [7], the series compensation topology is applied in both primary and secondary sides. The circuit topology diagram of the WPT system based on the MPRI with the cascaded ICTs is shown in Fig. 1. $U_{dc}$ represents the DC input voltage of the MPRI. The MOSFETs ($\mathbf{S}_{1a}$/$\mathbf{S}_{1b}$, $\mathbf{S}_{2a}$/$\mathbf{S}_{2b}$,$\cdots$, and $\mathbf{S}_{na}$/$\mathbf{S}_{nb}$) comprise the $n$-phase circuit in the MPRI ($n \geq 2, n \in \mathbf{N}$). $u_1$, $u_2$,$\cdots$, $u_n$ denote the fundamental components of the square-wave output voltage from each phase, respectively. $i_f$ is the fundamental component of the output current of the MPRI. $L_f$ is the extra compensation inductance in primary side. $C_f$ and $C_p$ are the compensation capacitor in primary side. $L_p$ and $R_p$ represent the inductance and the resistance of the primary coil, respectively. $L_s$ and $R_s$ are the inductance and the resistance of the secondary coil, respectively. $C_s$ is the compensation capacitor in secondary side. The series capacitors are applied to decrease the total impedance and increase the current through the series circuit. $M$ is the mutual inductance between the primary and the secondary coils. $R_L$ represents the load resistance. In this paper, the load resistance and the system frequency are fixed.

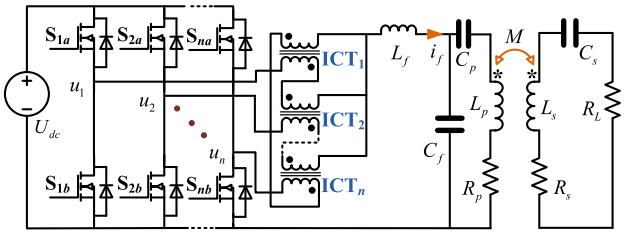


**FIGURE 1.** The circuit topology diagram of the WPT system based on the MPRI with the cascaded ICTs.

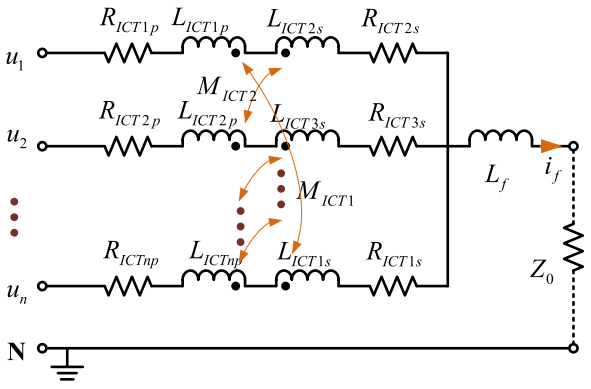


**FIGURE 2.** The equivalent circuit of the MPRI with ICTs.

The equivalent circuit of the MPRI with ICTs is shown in Fig. 2. $L_{ICT1p}$, $L_{ICT2p}$,$\cdots$, $L_{ICTnp}$ and $L_{ICT1s}$, $L_{ICT2s}$,$\cdots$, $L_{ICTns}$ represent the self-inductances in primary side and secondary of the ICTs (ICT$_1$, ICT$_2$,$\cdots$, ICT$_n$). $R_{ICT1p}$, $R_{ICT2p}$, $\cdots$, $R_{ICTnp}$ and $R_{ICT1s}$, $R_{ICT2s}$, $\cdots$, $R_{ICTns}$ represent the resistances in primary side and secondary of the ICTs. The impedances of the primary windings and the secondary windings in ICTs are denoted as $Z_{ICTkp} = R_{ICTkp} + j\omega L_{ICTkp}$ and $Z_{ICTks} = R_{ICTks} + j\omega L_{ICTks}$, $(k = 1, 2, \cdots, n)$ respectively. $\omega = 2\pi f$ and $f$ is the system operation frequency. The mutual inductance of the ICTs are $M_{ICT1}$, $M_{ICT2}$,$\cdots$, $M_{ICTn}$. $i_1, i_2,\cdots, i_n$ represent the fundamental components of the currents in each phase respectively. $Z_0$ is the equivalent load after the ICTs.

$U_k$ is the phasor of the fundamental component $u_k$ of the $k^{\text{th}}$ phase output voltage. $I_k$ is the phasor of the fundamental component $i_k$ in the $k^{\text{th}}$ phase circuit. $I_f$ is the phasor of $i_f$. Based on Kirchhoff's voltage law and current law, similar to [7], the equations of the circuit can be written as following:

$$\begin{cases} \mathbf{U}_1 = \left(Z_{ICT1p} + Z_{ICT2s}\right)\mathbf{I}_1 - j\omega M_{ICT1}\mathbf{I}_n \\ \qquad -j\omega M_{ICT2}\mathbf{I}_2 + \left(j\omega L_f + Z_0\right)\mathbf{I}_f \\ \mathbf{U}_2 = \left(Z_{ICT2p} + Z_{ICT3s}\right)\mathbf{I}_2 - j\omega M_{ICT2}\mathbf{I}_1 \\ \qquad -j\omega M_{ICT3}\mathbf{I}_3 + \left(j\omega L_f + Z_0\right)\mathbf{I}_f \\ \vdots \\ \mathbf{U}_n = \left(Z_{ICTnp} + Z_{ICT1s}\right)\mathbf{I}_n - j\omega M_{ICTn}\mathbf{I}_{(n-1)} \\ \qquad -j\omega M_{ICT1}\mathbf{I}_1 + \left(j\omega L_f + Z_0\right)\mathbf{I}_f. \end{cases} \tag{1}$$

$$\mathbf{I}_f = \sum_{k=1}^{n} \mathbf{I}_k. \tag{2}$$

In this paper, the ICTs are designed as identical. Hence, assuming that

$$\begin{cases} L_{ICTkp} = L_{ICTks} = L_{ICT} \\ R_{ICTkp} = R_{ICTks} = R_{ICT} \\ Z_{ICTkp} = Z_{ICTks} = Z_{ICT} = R_{ICT} + j\omega L_{ICT} \\ M_{ICTk} = M_{ICT}, \end{cases} \quad k = 1, 2, \cdots, n.$$

(1) can be simplified to

$$\begin{cases} \mathbf{U}_1 = 2Z_{ICT}\mathbf{I}_1 - j\omega M_{ICT}\mathbf{I}_2 - j\omega M_{ICT}\mathbf{I}_n \\ \qquad + \left(j\omega L_f + Z_0\right)\mathbf{I}_f \\ \mathbf{U}_2 = 2Z_{ICT}\mathbf{I}_2 - j\omega M_{ICT}\mathbf{I}_3 - j\omega M_{ICT}\mathbf{I}_1 \\ \qquad + \left(j\omega L_f + Z_0\right)\mathbf{I}_f \\ \vdots \\ \mathbf{U}_n = 2Z_{ICT}\mathbf{I}_n - j\omega M_{ICT}\mathbf{I}_1 - j\omega M_{ICT}\mathbf{I}_{(n-1)} \\ \qquad + \left(j\omega L_f + Z_0\right)\mathbf{I}_f. \end{cases} \tag{3}$$

After superposition, (3) can be written as

$$\sum_{k=1}^{n} \mathbf{U}_k = 2\left(R_{ICT} + j\omega L_{ICT} - j\omega M_{ICT}\right)\sum_{k=1}^{n} \mathbf{I}_k + n\left(j\omega L_f + Z_0\right)\mathbf{I}_f. \tag{4}$$

According to (2) and (4), the equation can be presented as

$$\sum_{k=1}^{n} \mathbf{U}_k = \left[2\left(R_{ICT} + j\omega L_{ICT} - j\omega M_{ICT}\right) + j\omega n L_f\right]\mathbf{I}_f + nZ_0\mathbf{I}_f. \tag{5}$$

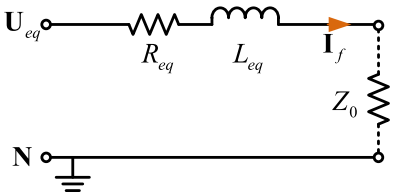


**FIGURE 3.** The equivalent single phase circuit of the MPRI with the ICTs.

(5) can be written as

$$\frac{1}{n}\sum_{k=1}^{n}\mathbf{U}_k = \left[\frac{2}{n}\left(R_{ICT} + j\omega L_{ICT} - j\omega M_{ICT}\right) + j\omega L_f\right]\mathbf{I}_f + Z_0\mathbf{I}_f. \quad (6)$$

The equivalent circuit of the MPRI with ICTs in Fig. 2 is equal to the equivalent single phase circuit in Fig. 3 according to (6). The equivalent resistance $R_{eq}$ and the equivalent inductance $L_{eq}$ are denoted as

$$L_{eq} = \frac{2}{n}\left(L_{ICT} - M_{ICT}\right) + L_f, \quad (7)$$

$$R_{eq} = \frac{2}{n}R_{ICT}. \quad (8)$$

$U_{eq}$, the phasor of the equivalent single phase output voltage $u_{eq}$ of the MPRI, is represented as

$$U_{eq} = \frac{1}{n}\sum_{k=1}^{n}U_k. \quad (9)$$

In [7], the expression of the equivalent single-phase output voltage in the complex domain is given without the detailed derivation process. In this paper, the construction method of iterative summation for trigonometric function is investigated to deduce the expression of the equivalent single phase output voltage about the number of phase and the maximum phase difference.

Similar to [7], assuming that the fundamental component $u_k$ of the $k^{\text{th}}$ phase output voltage is

$$u_k = \frac{2}{\pi}U_{dc}\sin\left(\omega t + \varphi_k\right), (k = 1, 2, \cdots, n), \quad (10)$$

where $\varphi_k$ is the phase angle of the $k^{\text{th}}$ phase output voltage.

The regulation of phase difference between adjacent phases is equally-spread in this paper as

$$\varphi_k = \frac{k-1}{n-1}\phi - \frac{1}{2}\phi = \frac{k}{n-1}\phi - \left(\frac{1}{n-1} + \frac{1}{2}\right)\phi, \quad (11)$$

where $\phi$ represents the maximum phase difference (namely, the phase difference between the first phase and the last phase).

According to (9), (10) and (11), $u_{eq}$ can be written as

$$u_{eq} = \frac{2U_{dc}}{n\pi}\sum_{k=1}^{n}\sin\left(\omega t + \frac{k}{n-1}\phi - \left(\frac{1}{n-1} + \frac{1}{2}\right)\phi\right). \quad (12)$$

Denoting $\theta_1 = \omega t - \left(\frac{1}{n-1} + \frac{1}{2}\right)\phi$ and $\theta_2 = \frac{1}{n-1}\phi$, (12) is equal to

$$u_{eq} = \frac{U_{dc}}{n\pi}\sum_{k=1}^{n}2\sin\left(\theta_1 + k\theta_2\right). \quad (13)$$

When $\phi = 0$, the RMS value of the equivalent single phase output voltage $U_{eq} = \frac{\sqrt{2}U_{dc}}{\pi}$.

When $\phi \neq 0$, the following trigonometric equation is constructed to calculate (13).

$$\cos\left(\theta_1 + \left(k - \frac{1}{2}\right)\theta_2\right) - \cos\left(\theta_1 + \left(k + \frac{1}{2}\right)\theta_2\right) = 2\sin\left(\frac{1}{2}\theta_2\right)\sin\left(\theta_1 + k\theta_2\right). \quad (14)$$

(14) is equal to

$$2\sin\left(\theta_1 + k\theta_2\right) = \frac{\cos\left(\theta_1 + \left(k - \frac{1}{2}\right)\theta_2\right) - \cos\left(\theta_1 + \left(k + \frac{1}{2}\right)\theta_2\right)}{\sin\left(\frac{1}{2}\theta_2\right)}. \quad (15)$$

According to (15), (13) can be written as

$$u_{eq} = \frac{U_{dc}}{n\pi} \times \frac{\cos\left(\theta_1 + \frac{1}{2}\theta_2\right) - \cos\left(\theta_1 + \left(n + \frac{1}{2}\right)\theta_2\right)}{\sin\left(\frac{1}{2}\theta_2\right)}, \quad (16)$$

where $\theta_1 + \frac{1}{2}\theta_2$ equals to $\omega t - \frac{n}{2(n-1)}\phi$ and $\theta_1 + \left(n + \frac{1}{2}\right)\theta_2$ equals to $\omega t + \frac{n}{2(n-1)}\phi$.

The expression of the equivalent single phase output voltage $u_{eq}$ as a function of the number of phases and the maximum phase difference can be deduced as

$$u_{eq} = \frac{U_{dc}}{n\pi} \times \frac{\cos\left(\omega t - \frac{n}{2(n-1)}\phi\right) - \cos\left(\omega t + \frac{n}{2(n-1)}\phi\right)}{\sin\left(\frac{1}{2}\theta_2\right)} = \frac{2U_{dc}}{n\pi} \times \frac{\sin\left(\frac{n}{2n-2}\phi\right)}{\sin\left(\frac{1}{2n-2}\phi\right)}\sin\left(\omega t\right). \quad (17)$$

The RMS value of the equivalent single phase output voltage can be written as

$$U_{eq} = \frac{\sqrt{2}U_{dc}}{n\pi} \times \frac{\sin\left(\frac{n}{2n-2}\phi\right)}{\sin\left(\frac{1}{2n-2}\phi\right)} = \frac{U_0}{n} \times \frac{\sin\left(\frac{n}{2n-2}\phi\right)}{\sin\left(\frac{1}{2n-2}\phi\right)}, \quad (18)$$

where $U_0 = \frac{\sqrt{2}\,U_{dc}}{\pi}$.

In this paper, the adjustment method of the maximum phase difference $\phi$ is proposed to control the output voltage of the MPRI with ICTs. The characteristics of the normalized equivalent single-phase output voltage varying with the number of phases and the maximum phase difference are shown in Fig. 4. According to (18) and the results in Fig. 4, the matching relationship between the output voltage and the maximum phase difference $\phi$ is obtained. After processing

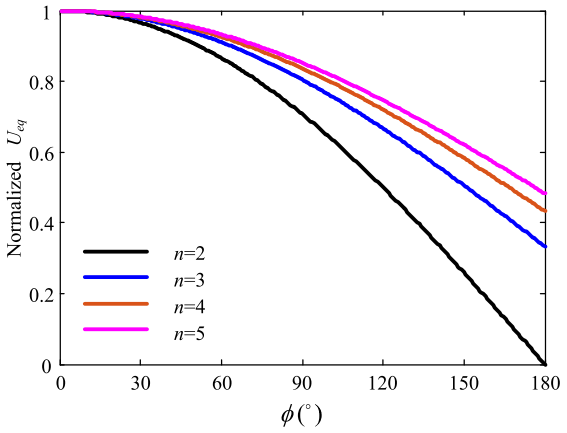


**FIGURE 4.** The characteristics of the normalized equivalent single phase output voltage varying with the number of phase and the maximum phase difference.

**TABLE 1.** A simplified look-up table.

| Normalized $U_{eq}$ | 1 | ⋯ | 0.95 | ⋯ | 0.90 | ⋯ | 0.80 | ⋯ |
|---|---|---|---|---|---|---|---|---|
| $\phi(^\circ)$ | 0 | ⋯ | 49.1 | ⋯ | 69.7 | ⋯ | 100.3 | ⋯ |
| Normalized $U_{eq}$ | 0.70 | ⋯ | 0.60 | ⋯ | 0.50 | ⋯ | | |
| $\phi(^\circ)$ | 124.8 | ⋯ | 146.4 | ⋯ | 166.5 | ⋯ | | |

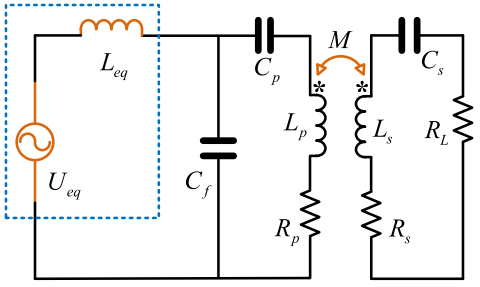


**FIGURE 5.** The equivalent circuit of the WPT system based on the MPRI with the cascaded ICTs.

the massive data of the matching relationship, a simplified look-up table of the matching relationship between the output voltage and the maximum phase difference $\phi$ is established in the inner process. The output voltage of the MPRI can be set to a certain value by adjusting the maximum phase difference $\phi$ according to the look-up table of the matching relationship. For example, when $n = 3$, a simplified look-up table with a few points to display the matching relationship as shown in Table 1.

## III. CIRCUIT MODELING OF THE WPT SYSTEM BASED ON THE MPRI WITH CASCADED ICTS

The equivalent circuit of the WPT system based on the MPRI with the cascaded ICTs is shown in Fig. 5, according to the equivalent single phase circuit of the MPRI of Fig. 3. The equivalent inner resistance $R_{eq}$ in the equivalent circuit is ignored due to $R_{eq} \ll \omega L_{eq}$.

In [24], the circuit model of the system with LCC compensation circuit is developed. Similarly, as shown in Fig. 5, the impedance of the secondary circuit is $Z_s = R_s + R_L + j\omega L_s + \frac{1}{j\omega C_s}$. When $C_s = \frac{1}{\omega^2 L_s}$, the secondary circuit resonates and $Z_s = R_s + R_L$. According to circuit theory of the mutual inductance, the reflected impedance from the secondary side to the primary side is $Z_r = \frac{(\omega M)^2}{Z_s} = \frac{(\omega M)^2}{R_s + R_L}$.

The total impedance in the primary circuit is

$$Z_p = j\omega L_{eq} + \frac{\left(\frac{1}{j\omega C_p} + j\omega L_p + R_p + Z_r\right)\frac{1}{j\omega C_f}}{\frac{1}{j\omega C_f} + \frac{1}{j\omega C_p} + j\omega L_p + R_p + Z_r}. \quad (19)$$

When $C_p$ and $C_f$ satisfy

$$C_f = \frac{1}{\omega^2 L_{eq}} = \frac{1}{\omega^2\left(\frac{2}{n}(L_{ICT} - M_{ICT}) + L_f\right)}, \quad (20)$$

$$C_p = \frac{1}{\omega^2\left(L_p - L_{eq}\right)} = \frac{1}{\omega^2\left(L_p - \frac{2}{n}(L_{ICT} - M_{ICT}) - L_f\right)}, \quad (21)$$

(19) is simplified as $Z_p = \frac{\omega^2 L_{eq}^2}{R_p + Z_r}$.

The output current of the MPRI is deduced as

$$\begin{aligned} I_f &= \frac{U_{eq}}{Z_p} = \frac{U_{eq}\left(R_p + Z_r\right)}{\omega^2 L_{eq}^2} \\ &= \frac{U_{eq}\left(R_p\left(R_s + R_L\right) + (\omega M)^2\right)}{\omega^2 L_{eq}^2\left(R_s + R_L\right)} \\ &= \frac{\sqrt{2}U_{dc}\left(R_p\left(R_s + R_L\right) + (\omega M)^2\right)\sin\left(\frac{n}{2n-2}\phi\right)}{n\pi\omega^2\left(\frac{2}{n}(L_{ICT} - M_{ICT}) + L_f\right)^2\left(R_s + R_L\right)\sin\left(\frac{1}{2n-2}\phi\right)}. \end{aligned} \quad (22)$$

The current in the primary circuit is

$$\begin{aligned} I_p &= \frac{U_{eq}}{j\omega L_{eq}} \\ &= \frac{\sqrt{2}U_{dc}\sin\left(\frac{n}{2n-2}\phi\right)}{jn\pi\omega\left(\frac{2}{n}(L_{ICT} - M_{ICT}) + L_f\right)\sin\left(\frac{1}{2n-2}\phi\right)}. \end{aligned} \quad (23)$$

According to the circuit theory of the mutual inductance, the current through the secondary side is

$$\begin{aligned} I_s &= \frac{j\omega M I_p}{R_L + R_s} = \frac{M U_{eq}}{L_{eq}\left(R_L + R_s\right)} \\ &= \frac{\sqrt{2}MU_{dc}\sin\left(\frac{n}{2n-2}\phi\right)}{\pi\left(2\left(L_{ICT} - M_{ICT}\right) + nL_f\right)\left(R_L + R_s\right)\sin\left(\frac{1}{2n-2}\phi\right)}. \end{aligned} \quad (24)$$

The receiving power is represented as

$$P = I_s^2 R_L = \frac{M^2 U_{eq}^2 R_L}{L_{eq}^2 (R_L + R_s)^2} = \frac{2M^2 U_{dc}^2 R_L \left(\sin\left(\frac{n}{2n-2}\phi\right)\right)^2}{\pi^2 \left(2(L_{ICT} - M_{ICT}) + nL_f\right)^2 (R_L + R_s)^2 \left(\sin\left(\frac{1}{2n-2}\phi\right)\right)^2}. \quad (25)$$

The total loss power of the system is

$$P_{loss} = I_p^2 R_p + I_s^2 R_s = \frac{2U_{dc}^2 \left(\sin\left(\frac{n}{2n-2}\phi\right)\right)^2}{\pi^2 \left(2(L_{ICT} - M_{ICT}) + nL_f\right)^2 \left(\sin\left(\frac{1}{2n-2}\phi\right)\right)^2} \times \left(\frac{R_p}{\omega^2} + \frac{M^2 R_s}{(R_L + R_s)^2}\right). \quad (26)$$

The system efficiency is

$$\eta = \frac{I_s^2 R_L}{I_p^2 R_p + I_s^2 (R_L + R_s)} = \frac{\omega^2 M^2 R_L}{R_p (R_L + R_s)^2 + \omega^2 M^2 (R_L + R_s)}. \quad (27)$$

According to the formulas above, the output current of the MPRI and the receiving power vary with the number of phases, the maximum phase difference, and the mutual inductance between the primary and secondary coils. The current in the primary coil varies with the maximum phase difference. The system efficiency varies with the mutual inductance between the primary and secondary coils. In the WPT system with unfixed receiver position, the mutual inductance frequently changes which causes the fluctuations of the relevant system characteristics. Especially, the fluctuation of the receiving power caused by the variation of the receiving position can be offset by adjusting the maximum phase difference. The following sections will discuss it in detail.

## IV. FLEXIBLE POWER CONTROL FOR THE WPT SYSTEM WITH UNFIXED RECEIVING POSITION

### A. SYSTEM CONTROL TOPOLOGY

To realize the stabilization control of the receiving power for the WPT system with unfixed receiver position, the flexible power control strategy is proposed based on the online monitoring of the key parameters, the pre-calculation of the inner parameters, the prediction of several conditions, and the online learning.

The topology diagram of system control for the WPT system with unfixed receiver position is shown in Fig. 6. In the primary side, the high-frequency output current of the MPRI is converted to the high-frequency voltage through the current transformer. The DC voltage is obtained further after the amplifier circuit, the rectifier circuit and the voltage divider circuit. This DC voltage corresponding to the original high-frequency current is measured by an ADC (analog-digital conversion) module in the micro controller unit (MCU). In this paper, the parameters of the inductance and capacitors are designed at fixed frequency. The low power rate of the system in this paper will hardly influence the temperature of the components. The driving signals are generated by the field-programmable gate array (FPGA). Hence, the issue of the frequency offset is ignored in this paper.

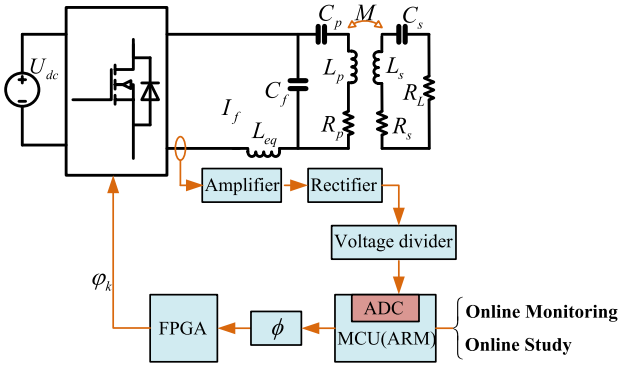


**FIGURE 6.** The topology diagram of system control for the WPT system with unfixed receiver position.

In the control process, the maximum phase difference $\phi$ is set in the MCU and sent to the FPGA (field-programmable gate array). The phase angles $\varphi_k$ of each phase are set to control the output voltage of the MPRI through the phase distribution program in the FPGA. Assuming that the output voltage of the MPRI is $U_{si}$ and the output current of the MPRI is $I_{fi}$ when the maximum phase difference $\phi$ is $\phi_i$, according to (22), the mutual inductance between the primary and secondary coils is derived as

$$M_i = \sqrt{\frac{L_{eq}^2 (R_s + R_L) I_{fi}}{U_{si}} - \frac{R_p (R_s + R_L)}{\omega^2}} = \sqrt{\frac{nL_{eq}^2 (R_s + R_L) I_{fi} \sin\left(\frac{1}{2n-2}\phi_i\right)}{U_0 \sin\left(\frac{n}{2n-2}\phi_i\right)} - \frac{R_p (R_s + R_L)}{\omega^2}}. \quad (28)$$

The maximum phase difference is put into it to show the relationship directly. Based on (28), the monitoring method of the mutual inductance between the primary and secondary coils is investigated to lay the foundation for the pre-calculation of the inner parameters in the next part.

### B. FLEXIBLE POWER CONTROL STRATEGY

According to the control conception mentioned above the flow chart of the flexible power control strategy including online monitoring and online learning is shown in Fig. 7.

*Step 1:* Setting arrays $I_f[i]$ and $\phi[i]$ for online learning parameters. In the system operation process, the selected data of the output current of the MPRI and the maximum phase

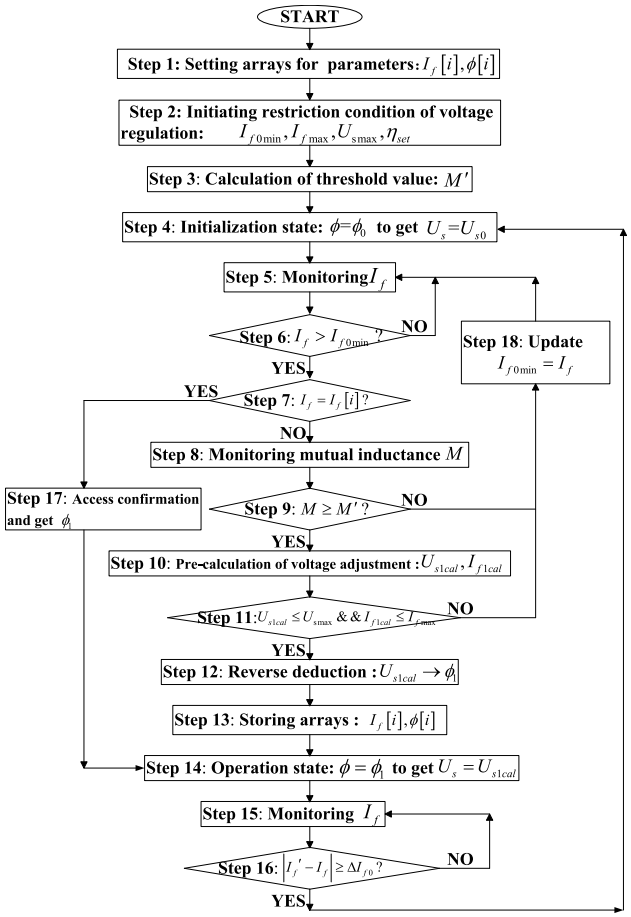


**FIGURE 7.** The flow chart of the flexible power control strategy for the WPT system with unfixed receiving position.

difference to adjust the output voltage are stored in the arrays $I_f[i]$ and $\phi[i]$ respectively.

*Step 2:* Initializing the threshold conditions of voltage regulation. The updatable global variable $I_{f0\min}$ is set as the minimum output current under initial $\phi = \phi_0$ when the system does not meet the threshold conditions of voltage regulation. $I_{f\max}$ is set as the permissible maximum output current of the MPRI. According to (18), $U_0$ is the maximum adjustable output voltage $U_{s\max}$ of the MPRI. The system efficiency should be more than $\eta_{set}$.

*Step 3:* Calculation of threshold value of the mutual inductance $M'$. In order to ensure that the system efficiency is more than $\eta_{set}$, according to (27), the threshold value $M'$ of the mutual inductance between the primary and secondary coils can be deduced as

$$M' = \sqrt{\frac{\eta_{set} R_p (R_L + R_s)^2}{\omega^2 (R_L - \eta_{set} (R_L + R_s))}}, \tag{29}$$

where $\eta_{set} < \frac{R_L}{R_L+R_s}$, $\frac{R_L}{R_L+R_s}$ is the efficiency of the secondary circuit.

*Step 4:* Initializing the system state. In initial state, the maximum phase difference is set as $\phi = \phi_0$. According to the matching relationship between the output voltage of the MPRI and the maximum phase difference, the initial output voltage of the MPRI is adjusted as $U_s = U_{s0}$.

*Step 5:* Monitoring the output current $I_f$ of the MPRI.

*Step 6:* Comparing $I_f$ with $I_{f0\min}$. If $I_f \leq I_{f0\min}$, misalignment of the receiver position at this time is larger than the misalignment of the stored learning example which does not meet the threshold conditions of voltage regulation. The receiver position this time does not meet the threshold condition. The system stays in the initiation state. The procedure jumps to Step 5 and the system continues monitoring $I_f$. If $I_f > I_{f0\min}$, the procedure jumps to Step 7.

*Step 7:* Searching in the stored array of the output current of the MPRI to check whether $I_f = I_f[i]$ or not. If $I_f = I_f[i]$, the procedure jumps to Step 17. If $I_f \neq I_f[i]$, the procedure jumps to Step 8.

*Step 8:* Calculating and monitoring of the mutual inductance. According to (28), the mutual inductance can be derived from $U_{s0}$ and $I_f$.

*Step 9:* Prediction of the mutual inductance. The calculated value of the mutual inductance in Step 8 is compared to the threshold value $M'$. If $M \geq M'$, the procedure jumps to Step 10. If $M < M'$, the system efficiency is lower than $\eta_{set}$ and the procedure jumps to Step 18.

*Step 10:* Pre-calculation of the voltage adjustment. In order to maintain the receiving power at $P_{set}$, according to (25), the output voltage of the MPRI needs to be adjusted to

$$U_{s1cal} = \sqrt{\frac{\omega^2 L_{eq}^2 (R_L + R_s) U_{s0} P_{set}}{\left(\omega^2 L_{eq}^2 I_f - U_{s0} R_p\right) R_L}}. \tag{30}$$

The corresponding output current $I_{f1cal}$ of the MPRI when the output voltage of the MPRI is $U_{s1cal}$ is deduced as

$$I_{f1cal} = \frac{U_{s1cal} I_f}{U_{s0}}. \tag{31}$$

According to (30) and (31), the theoretical values of the output voltage of the MPRI will be adjusted and the corresponding output current can be obtained.

*Step 11:* Prediction of the theoretical values of the output voltage to be adjusted and the corresponding output current. When $U_{s1cal} > U_0$ or $I_{f1cal} > I_{f\max}$, the threshold conditions of voltage regulation cannot be met and the procedure jumps to Step 18. When $U_{s1cal} \leq U_0$ and $I_{f1cal} \leq I_{f\max}$, the threshold conditions of voltage regulation can be met and the procedure jumps to Step 12.

*Step 12:* Reverse deduction of the maximum phase difference $\phi$. According to (18) and the results in Fig. 4, the matching relationship between the output voltage and the maximum phase difference $\phi$ is stored in the reverse deduction data table. The maximum phase difference $\phi_1$ corresponding with the calculated value $U_{s1cal}$ can be obtained based on this data table.

*Step 13:* The effective learning process is finished. The data $I_f$ and $\phi_1$ are stored in the arrays $I_f[i]$ and $\phi[i]$ respectively.

*Step 14:* Operation state. The maximum phase difference is selected as $\phi = \phi_1$ to achieve the output voltage $U_s = U_{s1cal}$.

*Step 15:* Monitoring the output current $I_f$ of the MPRI after the voltage regulation.

*Step 16:* Comparing the fluctuation $\left|I_f' - I_f\right|$ of the output current with the maximum allowable fluctuation $\Delta I_{f0}$. When $\left|I_f' - I_f\right| < \Delta I_{f0}$, the procedure jumps to Step 15 and the system continues to monitoring $I_f$. When $\left|I_f' - I_f\right| \geq \Delta I_{f0}$, the procedure jumps to Step 4 and the system jump to the initiation state.

*Step 17:* Reading the corresponding maximum phase difference $\phi_1$ from the stored arrays of the online learning. The procedure jumps to Step 14. In this paper, online learning means that storing the related parameters including the measured value and the setting value after every successful power stabilization control. In the next time, the stored parameters from the online learning will serve for the Searching and checking process in Step 7.

*Step 18:* The threshold conditions of voltage regulation cannot be met. The global variable $I_{f0\min}$ is updated as $I_{f0\min} = I_f$. The procedure jumps to Step 5.

To deal with the issue of the fluctuating receiver power caused by frequent changes of the receiver position, the flexible power control strategy is proposed in this paper. The recognition of load access and exit and the power stabilization control after access are realized according to this strategy when the load is at the new receiving position. The database of the online learning is established and updated during the system operation. When the load is at the previous receiving position or the position of the same mutual inductance, the parameter values are the same as the stored data and the maximum phase difference will be adjusted directly to control the output voltage of the MPRI according to the corresponding data. The proposed strategy effectively responds to those situations including load access, load exit, second and subsequent multiple movements of the load.

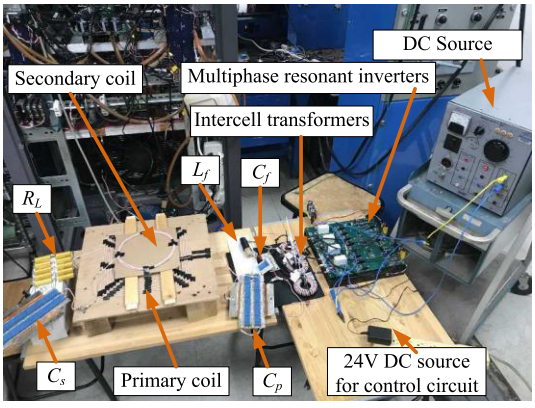


**FIGURE 8.** The experimental prototype of the wireless power transmission system with unfixed receiving position.

## V. EXPERIMENTAL VALIDATION

In order to verify the proposed flexible power control, an experimental prototype of the wireless power transmission system with unfixed receiver position is built as shown in Fig. 8. The number of the phases of the MPRI is 3 in this paper. The micro controller unit (MCU, STM32F407VGT) and field-programmable gate array (FPGA, XC6SLX9) are used in the control circuit of the MPRI. MOSFETs (IRFP4227) are utilized as the switching devices in the power stage circuit of the MPRI. The input of the MPRI is a DC voltage source. The ICTs are comprised of the core (T300-2) and the litz wire (14 AWG). Each ICT includes two identical windings in which the number of turns is 30. The inductance of the single winding in the ICT is 11.2 $\mu$H, measured by using a precision LCR meter (QuadTech 7600) at 85 kHz. The mutual inductance between the two windings of the ICT is 10.3 $\mu$H. The RMS value of the output voltage of each phase in the three-phase Class-D resonant inverter is set as 18 V by adjusting the DC voltage source. The theoretical output voltage of the MPRI is 18 V when the maximum phase difference is zero.

**TABLE 2.** System parameters.

| Parameters | Value |
|---|---|
| Output voltage of each phase circuit | 18 V |
| System operation frequency | 85 kHz |
| Inductance of the primary coil | 20.1 μH |
| Resistance of the primary coil | 60 mΩ |
| Inductance of the secondary coil | 21.7 μH |
| Resistance of the secondary coil | 30 mΩ |
| Load resistance | 4.2 Ω |

**TABLE 3.** The experimental parameters of the compensation circuits.

| Parameters | Calculated value | Measured value |
|---|---|---|
| $C_f$ | 701.2 nF | 700.5 nF |
| $C_p$ | 232.2 nF | 231.7 nF |
| $C_s$ | 161.8 nF | 161.1 nF |

The primary coil is a square spiral coil. The maximum side length is 30 cm. the number of turns is 7. The distance between the adjacent turns of every coil is 1 cm. The secondary coil is a circular spiral coil. The diameter is 20 cm and the number of turns is 7. The other parameters are listed in Table 2. To design $L_{eq}$ =5.0 $\mu$H in the primary compensation circuit, according to (7), the actual value of $L_f$ should be selected as 4.4 $\mu$H. $C_f$ is 700.5 nF (the calculated value is 701.2 nF) and $C_p$ is 231.7 nF (the calculated value is 232.2 nF). $C_s$ is 161.1 nF (the calculated value is 161.8 nF). The experimental parameters of the compensation circuits are listed in Table 3.

In this system, the high-frequency output current of the MPRI is converted to the high-frequency voltage through the current transformer in which the turns ratio of the current transformer is 1:50. After the amplifier circuit, the rectifier circuit and the voltage divider circuit, the DC voltage matching with the original high-frequency current is obtained. The DC voltage is measured by an analog-digital conversion module in the micro controller unit. Hence, the variation characteristic of output current of the MPRI is monitored.

To verify the proposed flexible power control strategy, the threshold values or the target values including the maximum output voltage of the MPRI, the maximum output

current of the MPRI, the minimum system efficiency and the receiving power are set first. The maximum output voltage of the MPRI $U_{s\max}$ is 18 V. The maximum output current of the MPRI $I_{f\max}$ is 10 A. The minimum system efficiency $\eta_{set}$ is 80%. The planned receiving power $P_{set}$ is 60 W.

In the initiation state, the maximum phase difference is set as $\phi = 154°$ according to the proposed strategy. The output voltage of the MPRI is 8.8 V. When the movable load is far away from the effective wireless charging area, the system maintains the initiation state if the threshold conditions of voltage regulation cannot be met. During the process of the load moving to the effective wireless charging area, the load voltage improves due to the increasing mutual inductance between the primary and secondary coils. The threshold conditions of voltage regulation are satisfied when the mutual inductance increases further. For the first time of the load access, according to the proposed control strategy, the system control process including the online monitoring method of the key parameters, the pre-calculation of the inner parameters, the prediction of several conditions and the online learning are carried out successively. The maximum phase difference is adjusted to $\phi = 0°$. The output voltage of the MPRI is 17.7 V. The load voltage is 15.8 V. The receiving power is 59.4 W. the system efficiency is 81.3%. The waveforms are tested by using the digital oscilloscope (RIGOL DS1074B) and the differential probe (PROBE MASTER Model 4231). All oscilloscope channels are set to 20V/div in this paper.

The position of the secondary coil is changed slowly and continuously for the second and subsequent multiple movements of the load. The amplitude of movement is 1.5 cm approximately. In the experimental part, the threshold value of the output current fluctuation of the MPRI for recognition of the load movement is set as 0.3 A. When the output current fluctuation is larger than 0.3 A, the load movement is tested by the system controller according to the proposed strategy. The maximum phase difference is adjusted to $\phi = 154°$ as the initiation state. In the initiation state, the output current of the MPRI is monitored. After searching in the stored array of the output current of the MPRI, the load position is stored in the database of online learning if $I_f = I_f[i]$. The maximum phase difference is adjusted directly to control the output voltage of the MPRI according to the corresponding data. If $I_f \neq I_f[i]$, the system will be controlled as the first time of the load access. In the experimental part, five load movements are tested during the moving process due to the threshold value of the output current fluctuation of the MPRI. The waveforms of the output voltage of the inverter and the load voltage during access and multiple movement process of the load are shown in Fig. 9. The waveforms of multiple movements of the load are shown in Fig. 10 in detail.

The experimental results, including the maximum phase difference, the output current of the MPRI, the load voltage, and the receiving power are listed in Table 4. The receiving power is controlled around the planned receiving power 60 W according to the proposed strategy. The deviation of the receiving power is less than 4%. As shown in TABLE 3,

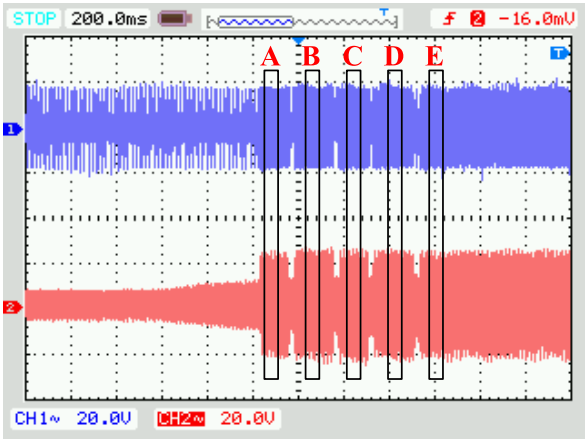


**FIGURE 9.** The waveforms of the output voltage of the inverter and the load voltage during multiple movement process of the load. Channel 1 (the output voltage of the inverter). Channel 2 ( the load voltage).

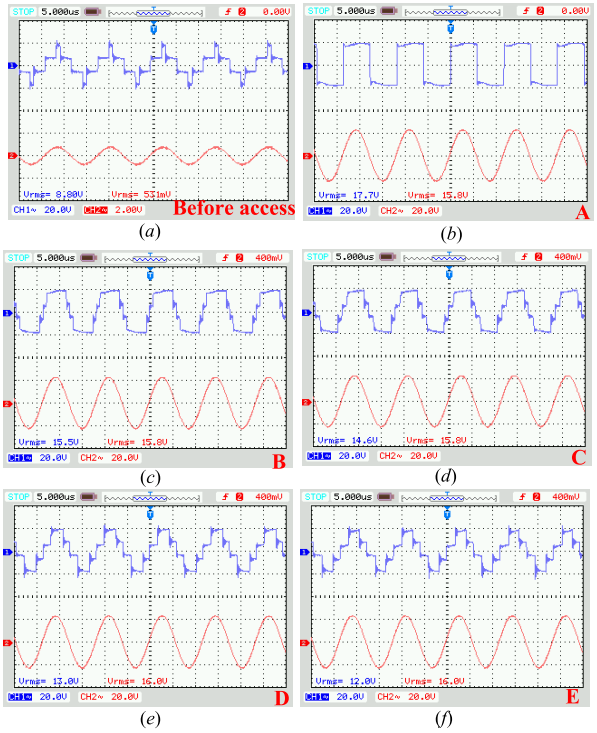


**FIGURE 10.** The waveforms of multiple movement of the load. (a) The waveforms before load access. Channel 1 (the output voltage of the inverter 8.8 V). Channel 2 ( the load voltage 0.53 V). (b) The waveforms of the A movement. Channel 1 (the output voltage of the inverter 17.7 V). Channel 2 (the load voltage 15.8 V). (c) The waveforms of the B movement. Channel 1 (the output voltage of the inverter 15.5 V). Channel 2 (the load voltage 15.8 V). (d) The waveforms of the C movement. Channel 1 (the output voltage of the inverter 14.6 V). Channel 2 (the load voltage 15.8 V). (e) The waveforms of the D movement. Channel 1 (the output voltage of the inverter 13.0 V). Channel 2 (the load voltage 16.0 V). (f) The waveforms of the E movement. Channel 1 (the output voltage of the inverter 12.0 V). Channel 2 (the load voltage 16.0 V).

during the variation of the receiving position (from **A** to **E**), the output voltage of the MPRI to maintain the stabilization of the receiving power decreases and the efficiency increases. During the position changing process in this experiment,

**TABLE 4. The experimental results during multiple movement process of the load.**

| Serial number of movements | A | B | C | D | E |
|---|---|---|---|---|---|
| Maximum phase difference (°) | 0 | 76 | 88 | 108 | 120 |
| Output voltage of the MPRI (V) | 17.7 | 15.5 | 14.6 | 13.0 | 12.0 |
| Load voltage (V) | 15.8 | 15.8 | 15.8 | 16.0 | 16.0 |
| Receiving power (W) | 59.4 | 59.4 | 59.4 | 61.0 | 61.0 |
| Efficiency (%) | 81.3 | 83.2 | 84.6 | 86.2 | 87.4 |

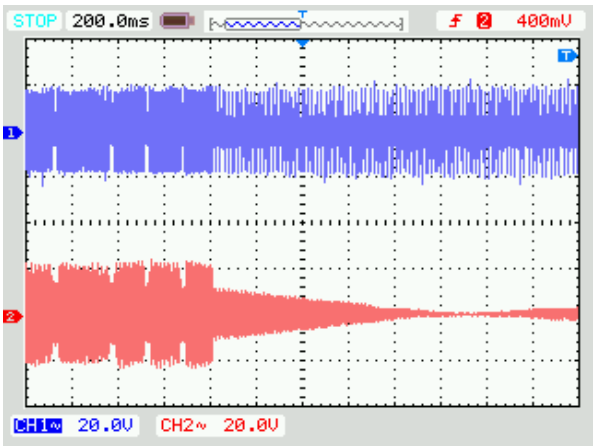


**FIGURE 11. The waveforms of the output voltage of the inverter and the load voltage during load exit process. Channel 1 (the output voltage of the inverter). Channel 2 (the load voltage).**

the mutual inductance (or the coupling coefficient) between the primary coil and the receiving coil increases. The results also fit in with this characteristic of the position changing process.

The exit process also includes several times of load movement. After the load moves far away from the effective wireless power transmission area, the controller continues to monitor the system characteristics. The threshold conditions of voltage regulation are not satisfied and the system maintains the initiation state. The waveforms of the output voltage of the inverter and the load voltage during load exit process are shown in Fig. 11.

The proposed flexible power control strategy for the WPT system with unfixed receiver position is verified by the experiments described above. Unlike other control methods, without the auxiliary positioning methods, the measuring in secondary side or the wireless communication between primary and secondary sides, the recognition of the load access and exit as well as the power stabilization control after access are achieved in this paper.

## VI. CONCLUSIONS

To deal with the issue of the fluctuation of the receiving power in the WPT system with unfixed receiver position, the flexible power control strategy is proposed in this paper. The theoretical analyses and the control strategy are validated by experiments and the conclusions are drawn as follows:

(1) Based on the circuit model of the MPRI with cascaded ICTs, an iterative summation method for trigonometric functions is presented to deduce the expression of the output voltage of the MPRI as a function of the number of phases and the maximum phase difference. The control method of the output voltage of the MPRI based on the adjustment of the maximum phase difference is proposed.

(2) Considering the cascaded ICTs and the LCC compensation circuit in the primary side, the design method of the compensation parameters is proposed based on the circuit model of the MPRI. The expressions for system parameters including the output current of the MPRI, the receiving power and the system efficiency versus the number of phases, the maximum phase difference and the mutual inductance are derived to lay the foundation of the control strategy.

(3) The system control topology for the flexible power control strategy including online monitoring and online learning is introduced. The online monitoring method of the mutual inductance between the primary and secondary coils is proposed according to the maximum phase difference, the number of the phase, and the output current of the MPRI.

(4) The flexible power control strategy including the online monitoring, parameter pre-calculation, prediction of several conditions, and the online learning is investigated for the wireless power transmission system with unfixed receiver position. The recognition of the load access and exit as well as the power stabilization control after access are achieved independent of the auxiliary positioning methods, the measurement in secondary side, or the wireless communication between primary and secondary sides.

## REFERENCES

[1] J. Moon, H. Hwang, B. Jo, H.-A. Shin, and S.-W. Kim, "Design of a 5-W power receiver for 6.78 MHz resonant wireless power transfer system with power supply switching circuit," *IEEE Trans. Consum. Electron.*, vol. 62, no. 4, pp. 349–354, Nov. 2016.

[2] J. Kim, H.-C. Son, D.-H. Kim, and Y.-J. Park, "Optimal design of a wireless power transfer system with multiple self-resonators for an LED TV," *IEEE Trans. Consum. Electron.*, vol. 58, no. 3, pp. 775–780, Aug. 2012.

[3] L. Li, H. Liu, H. Zhang, and W. Xue, "Efficient wireless power transfer system integrating with metasurface for biological applications," *IEEE Trans. Ind. Electron.*, vol. 65, no. 4, pp. 3230–3239, Apr. 2018.

[4] D. Patil, M. K. McDonough, J. M. Miller, B. Fahimi, and P. T. Balsara, "Wireless power transfer for vehicular applications: Overview and challenges," *IEEE Trans. Transp. Electrific.*, vol. 4, no. 1, pp. 3–37, Mar. 2018.

[5] C. Zhang, D. Lin, N. Tang, and S. Y. R. Hui, "A novel electric insulation string structure with high-voltage insulation and wireless power transfer capabilities," *IEEE Trans. Power Electron.*, vol. 33, no. 1, pp. 87–96, Jan. 2018.

[6] J. H. Kim *et al.*, "Development of 1-MW inductive power transfer system for a high-speed train," *IEEE Trans. Ind. Electron.*, vol. 62, no. 10, pp. 6242–6250, Oct. 2015.

[7] M. Bojarski, E. Asa, K. Colak, and D. Czarkowski, "Analysis and control of multiphase inductively coupled resonant converter for wireless electric vehicle charger applications," *IEEE Trans. Transp. Electrific.*, vol. 3, no. 2, pp. 312–320, Jun. 2017.

[8] M. Fu, C. Zhao, J. Song, and C. Ma, "A low-cost voltage equalizer based on wireless power transfer and a voltage multiplier," *IEEE Trans. Ind. Electron.*, vol. 65, no. 7, pp. 5487–5496, Jul. 2018.

[9] Q. Zhu, M. Su, Y. Sun, W. Tang, and A. P. Hu, "Field orientation based on current amplitude and phase angle control for wireless power transfer," *IEEE Trans. Ind. Electron.*, vol. 65, no. 6, pp. 4758–4770, Jun. 2018.

[10] J.-G. Kim, G. Wei, M.-H. Kim, J.-Y. Jong, and C. Zhu, "A comprehensive study on composite resonant circuit-based wireless power transfer systems," *IEEE Trans. Ind. Electron.*, vol. 65, no. 6, pp. 4670–4680, Jun. 2018.

[11] Y. Liu, R. Mai, D. Liu, Y. Li, and Z. He, "Efficiency optimization for wireless dynamic charging system with overlapped DD coil arrays," *IEEE Trans. Power Electron.*, vol. 33, no. 4, pp. 2832–2846, Apr. 2018.

[12] S. Assawaworrarit, X. Yu, and S. Fan, "Robust wireless power transfer using a nonlinear parity–time-symmetric circuit," *Nature*, vol. 546, pp. 387–390, Jun. 2017.
[13] J. Park *et al.*, "A resonant reactive shielding for planar wireless power transfer system in smartphone application," *IEEE Trans. Electromagn. Compat.*, vol. 59, no. 2, pp. 695–703, Apr. 2017.
[14] L. Tan *et al.*, "Coordinated source control for output power stabilization and efficiency optimization in WPT systems," *IEEE Trans. Power Electron.*, vol. 33, no. 4, pp. 3613–3621, Apr. 2018.
[15] M. Bertoluzzo, G. Buja, and H. K. Dashora, "Lumped track layout design for dynamic wireless charging of electric vehicles," *IEEE Trans. Ind. Electron.*, vol. 63, no. 10, pp. 6631–6640, Oct. 2016.
[16] W. Li, H. Zhao, S. Li, J. Deng, T. Kan, and C. C. Mi, "Integrated LCC compensation topology for wireless charger in electric and plug-in electric vehicles," *IEEE Trans. Ind. Electron.*, vol. 62, no. 7, pp. 4215–4225, Jul. 2015.
[17] H. Liu, L. Tan, X. Huang, C. Yan, J. Guo, and W. Wang, "Primary topology selection and conversion in short-segmented on-road charging system for electrical vehicles," *IET Power Electron.*, vol. 10, no. 4, pp. 499–507, Mar. 2017.
[18] W. Zhong and S. Y. R. Hui, "Auxiliary circuits for power flow control in multifrequency wireless power transfer systems with multiple receivers," *IEEE Trans. Power Electron.*, vol. 30, no. 10, pp. 5902–5910, Oct. 2015.
[19] M. Bojarski, E. Asa, K. Colak, and D. Czarkowski, "A 25 kW industrial prototype wireless electric vehicle charger," in *Proc. IEEE Appl. Power Electron. Conf. Exposit. (APEC)*, Long Beach, CA, USA, Mar. 2016, pp. 1756–1761.
[20] Q. Deng, J. Liu, D. Czarkowski, M. Bojarski, E. Asa, and F. de Leon, "Design of a wireless charging system with a phase-controlled inverter under varying parameters," *IET Power Electron.*, vol. 9, no. 13, pp. 2461–2470, Oct. 2016.
[21] N. Y. Kim, K. Y. Kim, J. Choi, and C.-W. Kim, "Adaptive frequency with power-level tracking system for efficient magnetic resonance wireless power transfer," *Electron. Lett.*, vol. 48, no. 8, pp. 452–454, Apr. 2012.
[22] T. Diekhans and R. W. D. Doncker, "A dual-side controlled inductive power transfer system optimized for large coupling factor variations and partial load," *IEEE Trans. Power Electron.*, vol. 30, no. 11, pp. 6320–6328, Nov. 2015.
[23] J. Yin, D. Lin, C. K. Lee, T. Parisini, and S. Y. Hui, "Front-end monitoring of multiple loads in wireless power transfer systems without wireless communication systems," *IEEE Trans. Power Electron.*, vol. 31, no. 3, pp. 2510–2517, Mar. 2016.
[24] H. Liu *et al.*, "Dynamic wireless charging for inspection robots based on decentralized energy pickup structure," *IEEE Trans. Ind. Informat.*, vol. 14, no. 4, pp. 1786–1797, Apr. 2018.

**HAN LIU** received the B.S. and Ph.D. degrees in electrical engineering from Southeast University, Nanjing, China, in 2014 and 2019, respectively. From October 2017 to October 2018, he was a Visiting Scholar with New York University, Brooklyn, NY, USA. He is currently a Lecturer with the College of Energy and Electrical Engineering, Hohai University, Nanjing. His research interests include wireless power transfer, wireless charging applications, and high frequency power electronics.

**XUELIANG HUANG** (M'11) received the B.S., M.S., and Ph.D. degrees in electrical engineering from Southeast University, Nanjing, China, in 1991, 1994, and 1997, respectively. From 2002 to 2004, he held a postdoctoral position with the University of Tokyo. Since 2004, he has been a Professor with the Department of Electrical Engineering, Southeast University. He has authored four books, more than 150 articles, and more than 40 inventions. His research interests include novel wireless power transfer systems, analysis of electromagnetic field, applied electromagnetics, and intelligent electricity technology.

**DARIUSZ CZARKOWSKI** (M'97) received the M.S. degree in electronics from the AGH University of Science and Technology, Krakow, Poland, the M.S. degree in electrical engineering from Wright State University, Dayton, OH, USA, and the Ph.D. degree in electrical engineering from the University of Florida, Gainesville, FL, USA, in 1989, 1993, and 1996, respectively. In 1996, he joined the New York University Tandon School of Engineering, Brooklyn, NY, USA, where he is currently a Professor of electrical and computer engineering. He has co-authored the book *Resonant Power Converters* (Wiley-IEEE Interscience, 2011). His current research interests include power electronics and power distribution systems. He is an Associate Editor of the *International Journal of Power and Energy Systems*.

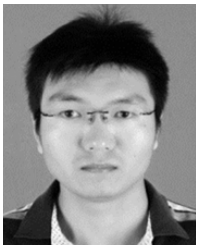

**LINLIN TAN** received the B.S. degree in electrical engineering and automation from Harbin Engineering University, Harbin, China, in 2008, and the Ph.D. degree in electrical engineering from Southeast University, Nanjing, China, in 2014, where he is currently a Lecturer with the School of Electrical Engineering. He has published more than 20 papers. His current research interests include wireless power transfer, wireless charging for electric vehicles, and wirelessV2G.

**JIACHENG LI** received the B.S. degree in electrical engineering from Southwest Jiaotong University, Chengdu, China, in 2015. He is currently pursuing the Ph.D. degree in electrical engineering with Southeast University, Nanjing, China. His research interest includes wireless power transfer.

**MING ZHANG** received the B.S. degree in electrical engineering and automation from Jiangsu Normal University, Xuzhou, China, in 2012, and the M.S. degree in electrical engineering from the Shanghai University of Electric Power, Shanghai, China, in 2015. He is currently pursuing the Ph.D. degree in electrical engineering with Southeast University, Nanjing, China. His research interests mainly include wireless power transfer technology and power electronics.

**ZHENXING ZHANG** received the B.S. degree from the School of Automation, Wuhan University of Technology, Wuhan, China, in 2016. He is currently pursuing the master's degree with the School of Electrical Engineering, Southeast University, Nanjing, China. His current research interests include wireless power transfer and wireless V2G.